A GENUINELY MULTIDISCIPLINARY JOURNAL

CHEMPLUSCHEM

CENTERING ON CHEMISTRY

Accepted Article

Title: Computer-aided design and synthesis of (1-(4-((3,4-dihydroxybenzylidene)amino)phenyl)-5-oxopyrrolidine-3-carboxylic acid) as a novel Nrf2 enhancer

Authors: Shirin Kahremany, Ilana Babaev, Pinhas Hasin, Tigist Tamir, Tali Ben-Zur, Guy Cohen, Sagiv Weintraub, Zhengyu Jiang, Daniel Offen, Ben Major, Shai Rahimipour, Hanoch Senderowitz, and Arie Gruzman

To be cited as: *ChemPlusChem* 10.1002/cplu.201700539

Link to VoR: http://dx.doi.org/10.1002/cplu.201700539

A Journal of

ChemPubSoc Europe

WILEY-VCH

www.chempluschem.org

Computer-aided design and synthesis of (1-(4-((3,4-dihydroxybenzylidene)amino)phenyl)-5-oxopyrrolidine-3-carboxylic acid) as a novel Nrf2 enhancer

Shirin Kahremany,[a] Ilana Babaev,[a] Pinhas Hasin,[a] Tigist Y. Tamir,[b] Tali Ben-Zur,[c] Guy Cohen,[d] Zhengyu Jiang,[e] Sagiv Weintraub,[a] Daniel Offen,[c] Shai Rahimipour,[a] M. Ben Major,[b] Hanoch Senderowitz,[a] Arie Gruzman*[a]

[a] Dr. S. Kahremany, Ilana Babaev, Dr. P. Hasin, Dr. S. Weintraub, Prof. S. Rahimipour, Prof. H. Senderowitz, Prof. A. Gruzman , Department of Chemistry, Faculty of Exact Sciences, Bar-Ilan University, Ramat Gan, 5290002 (Israel)
E-mail: gruzmaa@biu.ac.il

[b] Dr. Tigist Y. Tamir, Prof. M. Ben Major, Department of Pharmacology and the Lineberger Comprehensive Cancer Center, University of North Carolina at Chapel Hill, Chapel Hill, NC, 27599, (USA)

[c] Dr. T. Ben-Zur, Prof. D. Offen, Felsenstein Medical Research Center, Sackler Faculty of Medicine, Tel-Aviv University, Rabin Medical Center-Beilinson Campus, Petah Tikva 49100 (Israel)

[d] Dr. Guy Cohen, The Skin Research Institute. The Dead-Sea & Arava Science Center. Tamar regional council, Dead-Sea mobile post 86910, (Israel)

[e] Dr. Zhengyu Jiang, Jiangsu Key Laboratory of Drug Design and Optimization, Department of Medicinal Chemistry, School of Pharmacy, China Pharmaceutical University Nanjing, Jiangsu, (P. R. China)

Supporting information for this article is given via a link at the end of the document.

Abstract: We report on the design and synthesis of a novel nuclear factor erythroid 2-related factor 2 (Nrf2) enhancer. Using a structure-based virtual screening approach, we identified several commercially available compounds with high probability to interact with the Nrf2 binding pocket in the Kelch-like ECH-associated protein 1 (Keap1). Keap1 is an adaptor protein that recruits Nrf2 to a Cul3 (Cullin-3)-dependent ubiquitin ligase complex. The identified compounds were tested against rat pheochromocytoma PC-12 cells for their cytoprotective activity and one compound (SKT359126) demonstrated an Nrf2-mediated cell protective effect. Based on the SKT359126 structure, twenty-three novel derivatives were synthesized and evaluated. Among the screened derivatives, compound **16** (1-(4-((3,4-dihydroxybenzylidene)amino)phenyl)-5-oxopyrrolidine-3-carboxylic acid), demonstrated better activity than the parent molecules in activating the Nrf2 transduction pathway in a dose- and time-dependent manner. This compound can serve as a promising starting point for the development of novel therapeutics for the treatment of oxidative stress-related diseases.

1. Introduction

The human body is constantly exposed to numerous oxidative and electrophilic chemicals.[1] The imbalance between biochemical processes leads to the production of oxidative species that cause many human diseases.[2] The human antioxidant defense system is involved in the direct neutralization of these species.[3] The antioxidative system includes many enzymes, cofactors and vitamins.[4, 5] The activity of several antioxidant cytoprotective enzymes is controlled by the Nrf2/antioxidant response element (ARE) transcription pathway.[6] This pathway includes three main components: ARE, Nrf2 and Keap1.[7] The antioxidative response is initiated by Keap1. This protein is a cytoplasmic 624 amino-acid multi-domain protein that functions as a substrate adaptor protein to bring Nrf2 to a Cul3-dependent ubiquitin ligase complex. Keap1 contains (i) an N-terminal region (NTR, amino acids 1–60), (ii) a BTB (broad complex/tramtrack/bric-à-brac) proteins domain (amino acids 61–179)[8] through which Keap1 forms a homodimer and also interacts with Cul3, (iii) an intervening region (IVR, amino acids 180–314), which is cysteine-rich and contains eight cysteine residues among its 134 amino acids, (iv) a Kelch-domain made of six-bladed β-propeller in which each

blade of the propeller (I–VI) is composed of four β-strands (A–D) and (v) a C-terminal region (amino acids 599–624).[9-11]

Under physiological intracellular and environmental conditions, cytosolic Nrf2 is maintained at a low basal level by constitutive proteasomal degradation.[12] The specific binding of the Neh2 (Nrf2-ECH homology 2) regulatory domain of Nrf2 to Keap1[13] ensures the cytoplasmic sequestration and ubiquitination of Nrf2,[11, 14] thereby leading to Nrf2 proteasomal regulated degradation.[15] Keap1 has highly reactive thiol groups in its 27 cysteine residues causing the protein to be very sensitive to oxidative environments.[16]

Upon exposure to high levels of reactive oxygen species (ROS), Nrf2 is released from Keap1 and translocates into the nucleus.[15, 17] Inside the nucleus, the Nrf2 forms heterodimers with other basic leucine zipper domain (bZIP) transcription factors, including small Maf proteins, c-Jun, activating transcription factor-4, c-Fos, Fos-related antigen-1 (Fra-1) and *setera*.[18] These formed complexes bind to ARE in targeted gene promoters and upregulates their expression.[19] These genes [for example, glutathione S-transferases (GSTs), NADP(H), quinone oxidoreductase 1 (NQO1) and heme-oxygenase-1(HO1)] are critical for effective antioxidative stress response.

The Keap1 structure was used by our team as a basis for the molecular modeling of potential Nrf2 enhancers. Keap1 forms a homodimer, and each dimer binds one molecule of Nrf2, via its two Kelch domains, with one low-affinity (DLG motif, residues 24–31, latch) and one high-affinity binding site (ETGE motif, residues 78–82, hinge).[20]

Although the crystal structures of full Nrf2 or full Nrf2-Keap1 complex is not available yet, the crystallographic structures of the Keap1 Kelch domain in the presence of short peptides containing conserved ETGE and DLG motifs located in the Neh2 domain of Nrf2 have been solved.[21]

Despite the difference in the binding affinity, both the ETGE and DLG peptides display electrostatic interaction with Arg415 and Arg483 of Keap1, indicating the significant contribution of these residues to Nrf2 recognition. Therefore, both interaction sites were used as targets for Nrf2 activator design.[22-26] We hypothesized that binding of a small molecule to Keap1 instead of Nrf2 will prevent the binding of Keap1 to Nrf2 and therefore increase the nuclear concentration of the latter. The first inhibitor of the Nrf2–Keap1 protein−protein interaction (PPI) was developed by Wells group at 2012.[27] Almost all known protein−protein interaction (PPI) inhibitors of the Nrf2–Keap1 complex have a negatively charged group (Figure 1). In most cases, a carboxylic acid moiety or its isosteres have been used.[22] To date, compounds that belong to tetrahydroisoquinolines, sulfonamides, oxadiazoles, thiopyrimidines and furancarbazones have been reported as Keap1–Nrf2-interaction inhibitors.[22-26]

Covalent electrophilic Keap1 inhibitors that bind to thiol residues have been also reported.[28] However, these compounds have the potential to react with other cysteine moieties in different proteins and may therefore cause unpredictable side effects. Thus, the development of PPI inhibitors of the Nrf2–Keap1 complex is a most promising route.

Here we describe the design and synthesis of compound **16** that belongs to the oxopyrrolidine-based class of Nrf2 activators. The compound shows a cell-protective effect under severe oxidative stress conditions by activating the Nrf2 transduction pathway in a dose- and time-dependent manner. Nrf2 activators that belong to the oxopyrrolidine class of chemical compounds have not been described yet. Our prototype molecule can serve as a promising starting point for the development of novel therapeutics for the treatment of oxidative stress-related diseases.

2. Results and Discussion

The activity of Nrf2 is negatively regulated by binding to the Kelch domain of Keap1. Thus, compounds that interact with the Kelch domain and disrupt Nrf2 binding lead to the intracellular release of Nrf2. Free Nrf2 translocates to the nuclei and constantly activates the transcription of many antioxidant genes. As mentioned above, interactions between Keap1 and Nrf2 are mediated through the ETGE motif to a much greater extent than through the DLG one. Thus, we decided to focus on the ETGE motif as a target for the design of a competitive ligand that is able to release Nfr2. Based on the available crystal structures of the human Keap1 Kelch domain, as well as on the 16-mer-Nrf2 ETGE peptide (PDB codes 1ZGK and 2FLU, respectively) a pharmacophore model was therefore generated using the LigandScout software package[29] and used to identify features for potential small-molecule inhibitors of the Keap1−Nrf2 PPI. However, due to the large size of the Keap1-Nrf2 interface, the resulting model was found to be very complex to fit the size of small molecules. Thus, to adjust the model, we omitted two negative and one hydrophobic feature, based on visual inspection. The resulting pharmacophore presented in Figure 2 contains three negatively charged features, one hydrogen bond donor feature, a hydrophobic center, and 15 excluded volumes reflected potential steric restriction and corresponded to the

positions that are sterically claimed by the macromolecular environment surrounding the 16-mer-Nrf2 ETGE peptide.

This pharmacophore model was applied to virtual screening using the ZINC database.[30] A total of 7,377,031 (which are in stock) compounds were retrieved and processed using the Screen Library protocol, as implemented in LigandScout.[29] Based on this protocol, 25 conformations were generated for each compound. These conformations were subsequently fitted into the pharmacophore model using the LigandScout default parameters. Only 509 hits were obtained based on the features defined as essential (negative charge features), which constitute the basis for salt bridge formation. Five compounds with the highest binding score were selected for purchase (Figure 3).

As discussed earlier, Keap1−Nrf2 ETGE interacts via the formation of an electrostatic interactions network between conserved arginine (Arg380, Arg415 and Arg483) residues of Keap1 and acidic residues of the Nrf2 ETGE motif. In order to examine the ability of these five compounds to fit into the Keap1 binding site and to form these crucial interactions, they were first energy minimized and then flexibly docked into an energy-minimized Keap1 structure using Glide. The binding scores of the five top compounds are presented in S.Table 1 in the Supplemental Information.

The docking site was chosen according to the position of the peptide ligand cocrystallized at the binding site of Keap1 (PDB code: 2FLU). The results are summarized in Figure 4 and show that all five compounds were able to dock into the site by forming interactions with the conserved arginine binding site residues, similar to those formed by the Nrf2 ETGE motif, suggesting that they may potentially inhibit the Keap1–Nrf2 interaction.

These five molecules were purchased and biologically evaluated in PC-12 cells. This cell line derives from the neural crest of the pheochromocytoma of rat adrenal medulla of embryonic origin, which has a mixture of neuroblastic and eosinophilic cells.[31] Thus, these cells could easily differentiate into neuron-like cells even though they are not considered adult neurons. As a result, this model is used for screening the possible neuron-related biological effects of test compounds.[32-34] In our case, we used them as a general model for cellular oxidative stress.

The potential cytoprotective effect of the test compounds on the cell viability following a 24-h incubation period was investigated. Oxidative stress was induced by H_2O_2 at a concentration of 150 µM. Compounds and H_2O_2 were added simultaneously. Figure 5 shows that three out of the five tested compounds (MCULEPO1277, SKT656274 and SKT359126) were able to prevent the cytotoxic effect of H_2O_2 in the PC-12 cells. Cell viability increased by 40-50% for compounds MCULEPO1277, SKT656274 and SKT359126.

To prove that the cytoprotective effect of the compounds mediated through Nrf2 activation, a Dual-Luciferase Reporter Assay was conducted.[35] This assay is based on measuring the intracellular signal from two individual reporter enzymes within a single system. In the assay, the activities of the firefly and renilla luciferases are measured sequentially. Using this method, the direct activation of the promoter in PC-12 cells, which is usually activated by Nrf2, can be tested. As shown in Figure 6, only one out of three test compounds (SKT359126) significantly activates the Nrf2 promoter at the low pharmacological concentration of 10 µM. These results were further confirmed by the positive effect of the known Nrf2 activator tert-butylhydroquinone (tBHQ).[36]

Interestingly, the three-cyclic molecule SKT359126 was found to be active, whereas compound LTOO724252, in which two rings were replaced by a linear moiety, was found to be inactive. This fact emphasizes the importance of molecular rigidity for the biological activity. We hypothesized that the interaction between the negative charge of the carboxylic acids (SKT359126) and the positively charged arginines in the active center of Keap1 are stabilized by the rigid structure of the molecule. Thus, only the derivatives of compound SKT359126 were designed and synthesized.

In total, 23 novel derivatives of compound SKT359126 were designed, based on two parameters: 1) the existence of negatively charged moieties in the distal part of the molecules and 2) the structure's similarity to the parent compound. SKT359126 is commercially available and its synthesis was described by Paytash *et al.* in 1950. Based on this study, we synthesized nine of its amide pyrrolidine derivatives, as outlined in Scheme 1.[37] We did not applied a chiral control in the synthesis and also chiral resolution was not used. Thus, all compounds were a mixture of 4 diastereomers. The cyclization of *p*-phenylenediamine with itaconic acid resulted in a corresponding dicarboxylic-acid derivative.[37] Refluxing of SKT359126 with appropriate amines in dry DMF in the presence

of carbonyldiimidazole (CDI) yielded its novel amide derivatives, namely, 1,1'-(1,4-phenylene)bis(5-oxo-N-(thiazol-2-yl)pyrrolidine-3-carboxamide) **1**, 1,1'-(1,4-phenylene)bis(N-(5-methyl-1,3,4-thiadiazol-2-yl)-5-oxopyrrolidine-3-carboxamide) **2**, 1,1'-(1,4-phenylene)bis(N-(3-(1H-imidazol-1-yl)propyl)-5-oxopyrrolidine-3-carboxamide) **3**, 1-(4-(4-((3-(1H-imidazol-1-yl)propyl)carbamoyl)-2-oxopyrrolidin-1-yl)phenyl)-5-oxopyrrolidine-3-carboxylic acid **4**, (3-hydroxybenzyl)-1-(4-(4-((4-hydroxybenzyl)carbamoyl)-2-oxopyrrolidin-1-yl)phenyl)-5-oxopyrrolidine-3-carboxamide **5**, 1-(4-(4-((4-ethoxyphenyl)carbamoyl)-2-oxopyrrolidin-1-yl)phenyl)-5-oxopyrrolidine-3-carboxylic acid **6**, 1,1'-(1,4-phenylene)bis(4-(morpholine-4-carbonyl)pyrrolidin-2-one) **7**, 2,2'-((1,1'-(1,4-phenylene)bis(5-oxopyrrolidine-1,3-diyl-3-carbonyl))bis(azanediyl))bis(ethane-1-sulfonic acid) **8** and 5-oxo-1-(4-(2-oxo-4-(pyridin-3-ylcarbamoyl)pyrrolidin-1-yl)phenyl)pyrrolidine-3-carboxylic acid **9**. All these compounds are more extended than the parent compound. However, the binding site of Keap1 is known to be large enough to allow for proper interaction with the compounds.[38] Out of all the synthesized molecules, compounds **4**, **6** and **9** were obtained as monosubstituted ones, and were served as control compounds for testing the critical role of two negative charges/electron rich areas on the molecular skeleton. It is important to mention that, even without the second substitution, the molecule still has a negative charge, although at a shorter distance from the first negative moiety. In addition, we completely replaced the negatively charged and electron rich moieties by potentially two positively charged (in physiological conditions) domains in compound **3.** Finally, in compound **7** both negative charges were eliminated and replaced by a morpholine moiety. Both compounds: **3** and **7** were used as important controls for structure-activity relationships studies.

An additional diamide compound **10** with linear and aromatic substitutions in *p*-phenylenediamine was synthesised: (2-((4-(3-carboxyacrylamido)phenyl)carbamoyl)benzoic acid **10**. Briefly, *p*-phenylenediamine was reacted with phthalimide to afford the known intermediate 2-((4-aminophenyl)carbamoyl)benzoic acid. The obtained compound was reacted with furan-2-5-dione, resulting in **10**. Finally, two 2,4-dihydroxybenzoic acid were conjugated with *p*-phenylenediamine via amide bond formation, to obtain the symmetric compound ((1,4-phenylene)bis(2,4-dihydroxybenzamide) **11** (Scheme 2).

Moreover, in order to prevent free rotation and the formation of more rigid compounds, a double bond (imine) was introduced into the backbone of intermediate: 1-(4-aminophenyl)-5-oxopyrrolidine-3-carboxylic acid **12** to generate compounds **13**-**20**. This also decreases the length of the prepared compounds. The imine derivatives were synthesized as shown in Scheme 3. The first step of the synthesis was conducted in the same manner as described for the synthesis of amide pyrrolidine derivatives (Scheme 1). However, in this case, only the synthesis of the monosubstituted pyrrolidine molecule **12** was sufficient for the second substitution, and not the double substituted molecule (SKT359126). A new purification procedure was developed to obtain **12**. Briefly, the equivalent ratio between the itaconic acid and phenyldiamine was different from the ratio used for the synthesis of SKT359126. A ratio of 1:0.9 instead of 1:2 was used for the preparation of **12**. The compound was purified using several extraction and purification steps. First, using water at basic pH, unreacted itaconic acid and **12** were separated from the leftovers of the phenyldiamine. In the second step, by adding water at acidic pH, the itaconic acid and **12** were separated. Finally, using preparative HPLC, **12** was purified. The synthesis of **12** was also reported by Kolobov *et al.* and Rutkauskas *et al.*, [39-41] however they used a completely different synthetic strategy and purification methods with only 54% yields.

Compound **12** was used as a starting material for the synthesis of **13**–**20**. The appropriate aldehydes were coupled with **12** to obtain eight mixture of enantiomers of imine derivatives: 1-(4-((2,4-dihydroxybenzylidene)amino)phenyl)-5-oxopyrrolidine-3-carboxylic acid **13**, 1-(4-((4-carboxybenzylidene)amino)phenyl)-5-oxopyrrolidine-3-carboxylic acid **14**, 4-(((4-(4-(methoxycarbonyl)-2-oxopyrrolidin-1-yl)phenyl)imino)methyl)benzoic acid **15**, 1-(4-((3,4-dihydroxybenzylidene)amino)phenyl)-5-oxopyrrolidine-3-carboxylic acid **16** (only for this compound 2D NMR (NOESY) was conducted and the imine double bond configuration was determined as *E*), 1-(4-((3-hydroxybenzylidene)amino)phenyl)-5-oxopyrrolidine-3-carboxylic acid **17**, 1-(4-((2-hydroxybenzylidene)amino)phenyl)-5-oxopyrrolidine-3-carboxylic acid **18** and 1-(4-((3-carboxybenzylidene)amino)phenyl)-5-oxopyrrolidine-3-carboxylic acid **19**.

In addition, compound **12** was converted to the corresponding methyl ester to obtain methyl 1-(4-aminophenyl)-5-oxopyrrolidine-3-carboxylate, which was coupled with 4-carboxy benzaldehyde to yield compound **15**.

Two compounds (**14** and **19**) out of eight were prepared in the presence of a carboxylic acid moiety in both distal parts of the molecule. The rest of the imine analogs of SKT359126 were phenolic or polyphenolic molecules.

Compound **15** was prepared to investigate the role of the negative charge in the pyrrolidine domain. If the presence of such a moiety is critical for the biological activity, the elimination

of the negative charge in the pyrimidine part of the molecule is expected to reduce activity. The possible cytoprotective effect of all synthesized compounds was investigated on PC-12 cell viability. The ROS generation method was changed. Glucose oxidase (GO) was used this time as an inducer of the oxidative stress instead of the direct supply of H_2O_2.[42] We preferred to use a more tuneable and predictable system to generate H_2O_2 than its direct addition to the medium at a high dose. GO is a well-characterized ROS-generating system that continuously produces constant concentrations of H_2O_2 and O_2.[43] GO catalyses two electron reduction of oxygen to H_2O_2, using reducing equivalents from the oxidation of glucose to glycolic acid. Glucose is present in the medium at a high concentration. Therefore, the system never runs out of substrate for the enzymatic reaction. We also changed the order of addition of test compounds and ROS generation. In the first set of screening, H_2O_2 and compounds were added to the cells simultaneously, but in the second set of the experiments, compounds were suppled first to allow them to reach Nrf2-Keap1 complex and after then ROS were added to the experimental system. In this case, cells were already protected against oxidative stress, even before ROS attacked them. Cells were incubated for 2.5 h with the test compounds (1 and 10 µM) under physiological conditions and then further 1.5 h incubation under the oxidative stress environment. Cell survival was then determined by the MTT assay. Figure 7 shows that compound **16** exhibited a moderate but significant cell-protective effect at a concentration of 10 µM (17%), as compared to the control cells, treated by a the vehicle (containing 0.1%DMSO).

To verify that the effect of **16** is indeed pharmacologically relevant, dose- and time-dependent curves of its activity were generated. Figure 8A shows that **16** dose-dependently protects PC-12 cells under oxidative stress conditions. The minimal effective concentration was determined as 10 µM, as we already concluded from the screening experiments. The maximal effective concentration was 100 µM, and 40% cell protective effect was achieved. Two additional time points of the exposure to the compound **16** (6 h and 24 h) were added to the 4-h interval of cell incubation with H_2O_2, which was used in the screening experiments (Figure 8B). At this point, we were forced to replace the GO system, which we used for the 4-h incubation, by H_2O_2 (150 µM), due to massive cell death during longer incubation periods with GO. The effect of **16** at the lowest concentration (10 µM) at both time points was much larger than that at the same concentration after only 4 h (50–55% versus 17%). An identical cytoprotective effect (50–55%) was observed using 50 µM of **16**. Thus, we concluded that the maximal effective concentration of **16** depends on the time of incubation. After only 6 h, the maximal effective concentration of **16** was just 10 µM. The longer incubation time (24 h) only moderately increased the effect of **16** on the PC-12 viability.

An additional control experiment was conducted to determine whether the lead compound has a positive effect on cell proliferation. Such positive effect on the number of live cells in antioxidant experiments may mimic the increased cell viability, which we attributed to the antioxidant activity of compound **16**. A proliferation assay (following a 24-h exposure to **16** at a concentration of 50 µM) was performed with PC-12 cells using the MTT test (Figure 8C). These results proved that **16** has no significant effect on the proliferation rate of the cells and demonstrate that the observed antioxidant cellular effect of **16** is only related to its antioxidative properties.

Next, we evaluated the role of various moieties of **16** on its activity. First, the importance of the pyrrolidine ring and the catechol moiety for the biological activity was investigated. Compounds **20**-**22**, (hydroxybenzylidene)amino)phenyl)carbamoyl)benzoic acid **20**, 2-((4-((4-carboxybenzylidene)amino)phenyl)carbamoyl)benzoic acid **21** and 1-(4-((4-cyanobenzylidene)amino)phenyl)-5-oxopyrrolidine-3-carboxylic acid **22**, were synthesised by replacing the pyrrolidine ring in **16** by 2-(carbamoyl)benzoic acid, and the catechol moiety by either *p*-phenol in **20,** *p*-carboxylic acid in **21** or *p*-nitrile moiety in **22**. These three catechol replacements were chosen because of the similarity in terms of the partially negative charge (δ^-) on the catechol and nitrile or phenol groups. In the case of carboxylic acid, the molecule is negatively charged at the physiological pH due to anion formation. All three compounds were synthesized from 2-((4-aminophenyl)carbamoyl)benzoic acid, as shown in Scheme 4. Four-hydroxybenzaldehyde, 4-formylbenzoic acid, or 4-formylbenzonitrile were reacted with 2-((4-aminophenyl)carbamoyl)benzoic acid, respectively, to obtain the resulting compounds **20**, **21** and **22** (Scheme 4A).

Finally, compound **23** was synthesized from itaconic acid and commercially available 5-amino-2-(carboxymethyl)benzoic acid, to obtain a mixture of enantiomers as shown in Scheme 4B. By synthesizing and testing this molecule, we planned to determine the role of catechol moiety in the biological activity of **16**, by replacing the two phenolic hydroxyls by two carboxylic acids and eliminating the aromatic ring.

All four compounds were screened in PC-12 cells at two concentrations, 10 and 50 µM and their activity was compared to that of compound **16** (Figure 9). At 10 µM, all four compounds (**20**-**23**) failed to show significant protecting effect on the cell

viability, although compound **16** significantly protected PC-12 cells against oxidative stress at 10 μM. At a concentration of 50 μM, however, compound **20** (the molecule in which the catechol moiety was replaced by a phenol group and the carboxypyrollidine ring was changed to a carboxybenzyl cycle) exhibited significant protecting activity although its activity was considerably lower than that of compound **16** (17% versus 40%). Based on these results, we concluded that a tri-cyclic backbone, including an oxopyrrolidine ring substituted by carboxylic acid, phenylmethanimine and catechol moieties, are critical for the biological activity. The carboxylic acid and catechol are most likely responsible for the interaction with the Arg415 and Arg483 residues of Keap1. Remarkably, non-active compounds such as **11** and **21** do not have the oxopyrrolidine ring. In addition, the non-active compound **10** has an ester substitution on the oxopyrrolidine ring instead of free carboxylic acid. This difference may prevent the formation of salt bridges between the free carboxylic acid with arginine residues in the binding site of Keap1. Compound **19** has a phenol ring, in which the hydroxyl group is located at the *ortho* position relative to the iminic bond. This change may be crucial for the activity, because the distance between the hydroxyl group and the arginine residues of Keap1 is too short for the binding interaction to take place.

The catechol moiety is part of the structure of compound **16**, which is known for its direct antioxidant activity.[44] Thus, to evaluate whether the antioxidant activity of **16** is related to the activation of some intracellular mechanisms (we assumed that this is the Nrf2 activation) or direct quenching of ROS, the antioxidant activity of **16** was measured by the 2',7'-dichlorofluorescin (DCFH) method. In this method, the nonfluorescent DCFH is oxidized by a ROS, such as H_2O_2, to form fluorescent 2,7-dichlorofluorescein (DCF; excitation 485 nm, emission 535 nm)[45]. Besides compound **16**, four additional molecules were used as a control, including two monophenols (**18** and **20**), one polyphenols (**11**) and the molecule without the phenol moiety (**15**). All five compounds were inactive in the cell-protection assay. The concentration chosen for the DCFH assay was relevant to the observed biological effect (10 μM). Figure 10A shows that none of the five compounds reduced the oxidation of DCFH to DCF, indicating that the antioxidant effect of **16** in PC-12, is not related to their direct ability to quench ROS as could have been expected based on the presence of the phenolic or catechol moieties in four out of five molecules. Moreover, at the tested concentration, all five compounds with phenol moieties including **16**, which was active in the cellular assay showed no significant direct scavenger activity. In contrast known polyphenolic free radical scavenger tBHQ[46] showed moderate, but significant reduction of DCF signal starting from 10 μM concentration (Figure 10B).

Finally, the most important evidence showing that **16** induces an antioxidant effect via activating the Nrf2 pathway was obtained by examining the direct effect of the test compound on the rate of Nrf2 nuclear translocation, using commercially available kits as described in the Experimental part. Physiological activation of Nrf2 by ROS lead to translocation of the former from the cytosol to nuclei, where Nrf2 is activate transcription of antioxidant genes. Thus, increased amount of Nrf2 in PC-12 cellular nuclear fraction after expose the cells to **16** might be an indication for the induced by the compounds Nrf2 dissociation from Keap1. The nuclear fraction of treated by **16** and control cells were isolated and the activation of ARE was investigated by testing amount of Nrf2 in nuclear fractions by Nrf2-ARE binding kit as described in the Experimental part. This ELISA kit is measuring binding activity of Nrf2 to ARE immobilized sequence using sensitive colorimetric readout. The intensity of the signal is directly correlated with the amount of Nrf2 which interacted with ARE Nrf2. The amount of Nrf2 is depends on the translocation level of this protein to nuclei.

Compound **16** significantly increased the translocation of Nrf2 into the nucleus after 2 h of incubation (Figure 11A) without inducing the oxidative stress. Known Nrf2 inducer (Al-1) was used as a positive control.[47] These results indirectly support our hypothesis that compound **16** can interrupt Nrf2 interaction with Keap1 and increase its release from the complex without involving the main trigger of this process, oxidative stress. Interestingly, when cells pre-treated with **16** were exposed to GO, the compound also exhibited a stimulatory effect on the Nrf2 translocation (Figure 11B). It is worth mentioning that **16** is active in the absence of GO and that its effect is additive to that of the natural activator of the Nrf2 released from the Keap1 – ROS, when incubated together, suggesting that the mechanisms of Nrf2 activation by **16** and by ROS might be distinct. In another hand, this data does not necessarily suggest that the mode of action of ROS and **16** are separate - it is a possibility that they have additive effects acting via the identical mechanism (assuming neither **16** saturates the ROS activating mechanism). ROS causes the oxidation of thiol groups in Keap1, and this effect is the main trigger for the Nrf2 release and nuclear translocation.[12] Compound **16** was designed as an inhibitor of the Kelch domain binding site, which is responsible for Nrf2 binding. Such inhibition should lead to an increased non-binding fraction of Nrf2. Although, we did not prove the proposed mechanism in the molecular level, the activity of **16** in the absence of ROS may support our hypothesis that compound **16**

mediates its biological activity by direct stimulation of the Nrf2 pathway. In one hand, many Nrf2 enhancers are electrophilic (including polyphenols) that directly, or after metabolic activation bind to thiol residues in Keap1. Compound **16** is catechol and might be oxidized in the physiological environment. After such change, the molecule is able to induce Nrf2 activity by binding to electrophile response element.[48, 49] In another hand, two other polyphenols (compounds **11** and **13**) have not shown significant biological effect, despite the presence of the identical experimental conditions. Thus, based on this data, we at least partially might conclude that compound **16** activates Nrf2 via non-dependent to thiols interactions.

In addition, docking simulations suggest that compound **16** interacts with the arginine-rich area in the Kelch domain of Keap1 in the same mode as the Nrf2–ETGT motif (Figure 12). Analysis of the binding mode of **16** reveals that the interactions are hydrophobic and electrostatic. There are two π–π stacking interactions between the compound and protein sidechains: Tyr334 and Tyr572. Moreover, **16** forms several H-bonds with the side chains Arg415, Arg483, Ser508, Ser555 and Tyr334.

Thus, positive correlation between *in silico* modeling, the cell-protective effect and the subsequent nuclear translocation of Nrf2 caused by compound **16** indicates that its molecular mechanism is indeed through Nrf2 release.

Compound **16** may provide a structural basis for the development of more potent and effective Keap1–Nrf2 interaction inhibitors. It is important to mention that mimicking the ETGT–Nrf2 domain by a small organic molecule is a relatively novel approach that has attracted much attention over the past three years,[50] whereas the traditional approach is to target the thiol groups in Keap1 by covalent modifications. Further *in vivo* work is needed to determine whether compound **16** can be used as a drug candidate in severe human disorders related to oxidative stress, such as cancer, neurodegenerative diseases and diabetes.

LEGENDS

Figure 1. *Structure of known Keap1–Nrf2 PPI inhibitors.*

Figure 2. *Pharmacophore design*. *(A) Crystal structures of Keap1 and Nrf2 ETGE peptide (PDB code: 2FLU).* Residues depicted as sticks show the interaction of the Nrf2 ETGE side chain with Arg 380, 415 and 483 of Keap1. (B) Structure-based pharmacophore model generated with LigandScout from the crystal structure of the Nrf2 ETGE peptide and the Kelch domain of Keap1. *(C) The final pharmacophore which was used for screening.* Features are color-coded as follows: negative charge, red; hydrogen bond donor, green; hydrophobic center, yellow; excluded volumes, gray.

Figure 3. Virtual screening results. *(A) Structures of the top five compounds obtained from the virtual screening. (B) Fitting of the compounds to the pharmacophore model, 2D Binding mode interactions.* Features are color-coded, as described in Figure 2C.

Figure 4. *Docking of the five selected compounds at the Keap1 binding site and their 2D ligand interaction diagram.* Residues indicated by pink- and green-colored spheres represent electrostatic and van der Waals interactions, respectively. Hydrogen bonds are indicated by dashed lines.

Figure 5. *Screening of the five compounds with the highest fitting score for their cytoprotecting activity.* PC-12 cells were grown as described in the Experimental Section. The cells were exposed to 150 μM H_2O_2 and either to DMSO (**C**, 0.1%) or to the test compounds SKT716764 (SKT7), MCULEP01277 (1277), LTOO724252 (LTOO), SKT656274 (SKT6) and SKT359126 (SKT3). All compounds were added at a concentration of 10 μM.. After that, a standard MTT analysis was conducted after 24 h. *p ≤ 0.05, n = 3, mean±SE.

Figure 6. *Stimulatory effect of SKT3 on the Nrf2 promoter.* Three active compounds in the cell-protection assay: SKT3, SKT6 and 1277 and DMSO (**C**) were introduced into PC-12 cells at a concentration of 10 μM for 24 h. tBHQ (15 μM) was used as a positive control. A double luciferase method was applied, as described in the Experimental Section. *p ≤ 0.05, n = 3, mean±SE.

Figure 7. *Effect of synthesized compounds on PC-12 viability*. PC-12 cells were grown as described in the Experimental Section. The cells were incubated with the test compounds for 2.5 h at concentrations of 10 μM (black columns) and 1 μM (gray columns). After that, GO (250 mUnits per ml) was added for an additional 1.5-h incubation period. The control cells were treated by DMSO [red color columns (0.1%)]. A standard MTT analysis was conducted. *p ≤ 0.05, mean±SE (n = 3).

Figure 8. Pharmacological characterization of the lead compound. *(A) Dose-response analysis of the effect of **16***. PC-12 cells were grown and treated as described in Figure 7. *p ≤ 0.05, mean±SE (n = 3). (B) *Time-course analysis of the effect of **16***. The cells were initially exposed to increasing concentrations of **16**, from 10 to 50 μM, and then exposed to 150 μM H_2O_2 for 6 and 24 h. Following the exposure, a standard MTT analysis was conducted. *p ≤ 0.05, mean±SE (n = 3). (C) *Lack of effect of **16** on proliferation rate of PC-12.* Following exposure to **16** for 24 h at a concentration of 50 μM, a standard MTT analysis was conducted. n = 3.

Figure 9. *Dose-response analysis of the effect of **16** and its derivatives on PC-12 viability.* The cells were treated as previously described (Figure 7). They were then exposed to increasing concentrations of the compounds, 10 μM (red columns) and 50 μM (blue columns). DMSO was used as a control (0.1%, black color). After 4 h, MTT analysis was conducted as described in the Experimental Section. *p ≤ 0.05, mean±SE (n = 3).

Figure 10. *Lack of the DCF-scavenging effect of the test compounds*. (A). The test compounds were diluted at a ratio of 1:10 with 40 mM Tris (pH 7.4) to give 10 μM final concentration and then loaded with 10 μM of DCFH (in methanol) for 15 min at 37 °C. After exposure to a solution containing 30% H_2O_2, the formation of the fluorescent-oxidized derivatives of DCF was monitored in a cuvette holder (thermostatically maintained at 37 °C) as follows: DCF, excitation wavelength (488 nm) and

emission wavelength (525 nm). DCF formation was quantified from separate standard curves in methanol (0.05–1 lm). 0.1% DMSO was added in the control treatment. (B). Scavenging effect of tBHQ was compared with compound **16** in identical conditions which were described in panel A. The results are shown as the mean ± SE. Control cells were treated by DMSO (0.1%) *p < 0.05.

Figure 11. *Compound **16** activated the Nrf2 anti-oxidant system.* (A) PC-12 cells were incubated with 50 µM of **16** or Al-1 during 2 h and then nuclear extract was prepared using a commercially available nuclear extraction kit. The nuclear translocation of Nrf2 was quantified by the Nrf2 activity kit. (B) PC-12 cells were initially exposed to 50 µM of **16** for 2 h and then 300 µM of GO were added for additional 2 h. The induced nuclear translocation of Nrf2 was quantified by the Nrf2 activity kit. The results are shown as the mean ± SE. Control cells were treated by DMSO (0.1%) *p < 0.05.

Figure 12. *The binding mode between the active conformation of compound **16** and Keap1 provided by Glide docking.* (A) Keap1 surface with compound **16**. (B) 3D diagram of the interactions between compound **16** and the Keap1 binding site. Only interacting residues are displayed. H-bonds are displayed as dotted green arrows and the π–π stacking interactions as pink dashed arrows. (C) 2D diagram of the interactions between **16** and the Keap1 binding site. H-bonds are displayed as dotted green arrows.

Scheme 1. *Synthesis of nine novel amide pyrrolidine derivatives:* a) Benzene-1,4-diamine, 2-methylenesuccinic acid, H_2O, reflux 1 h. b) 1) CDI, dry DMF, 80 °C 1 h. 2) Reflux, 6–7 h.

Scheme 2. *Synthesis of **10*** and ***11**:* a) THF, RT 4 h. b) EtOH, aromatic aldehyde, RT overnight. c) Dry DMF, CDI, reflux 6 h. d) H_2O, reflux 1 h.

Scheme 3. *Synthesis of **13**–**19***: a) H_2O, phenylenediamine, itaconic acid reflux 1 h. b) EtOH, **12**, aromatic aldehyde, RT overnight. c) MeOH, H_2SO_4, reflux 5 h.

Scheme 4. *Synthesis of **20**–**23**:* a) THF, RT 4 h. b) EtOH, aromatic aldehyde, RT overnight. c) Dry DMF, CDI, reflux 6 h. d) H_2O, reflux 1 h.

3. Conclusions

Based on the crystal structure of the Keap1–Nrf2 peptide complex, a pharmacophore model was designed and, using virtual screening, five initial hits were chosen. Based on one of them, 1,1'-(1,4-phenylene)bis(5-oxopyrrolidine-3-carboxylic acid (SKT359126), 23 different novel derivatives were designed, synthesized and biologically evaluated. Compound 1-(4-((3,4-dihydroxybenzylidene)amino)phenyl)-5-oxopyrrolidine-3-carboxylic acid (**16**) exhibited an *in vitro* cell protective effect via the activation of the Nfr2 pathway.

Experimental Section

Materials

All chemical reagents, solvents, and acids were purchased from Acros Organic, Alfa Aesar, Bio-Lab Ltd., Merck, or IU-CHEM Ltd., and all were used as received. Analytical and preparative HPLCs (Young Lin Instruments, Anyang, Korea) were performed on LUNA C_{18} preparative (10 µm, 100ª30 mm) or analytical (5 µm, 250ª4.6 mm) columns, both from Phenomenex, Inc. (Torrance, CA, USA). HPLC purification was carried out with an increasing linear gradient of CH_3CN in H_2O. Purity of the synthesized compounds was confirmed by HPLC analysis. Analytical TLC was carried out on pre-coated silica gel 60 F_{254} (Merck) sheets using UV absorption and iodine physical adsorption for visualization. Mass spectra were recorded on a Finnigan Model 400 instrument using a QToF microspectrometer (Micromass, Milford, MA, USA), by electrospray ionization (ESI) in the positive/negative ion modes. The data were processed using mass LynX ver. 4.1 calculations and de-convolution software (Waters Corp., Milford, MA, USA). High-resolution mass spectra (HRMS) were obtained using an LTQ Orbitrap XL (Thermo Scientific, Waltham, MA, USA). Melting points were measured with a Fisher-Johns melting-point apparatus (Waltham, MA, USA). Elemental analysis was conducted using Thermo Flash 2000 CHN-O Elemental Analyzer (Waltham, Massachusetts, United States). β-Mercaptoethanol, Phenylmethanesulfonyl fluoride (PMSF), sodium orthovanadate, sodium-β-glycerophosphate and sodium pyrophosphate decahydrate were purchased from Alfa Aesar (Karlsruhe, Germany). Ethylene glycol-bis-N,N,N′,N′-tetraacetic acid tetrasodium salt (EGTA) was received from AppliChem (Darmstadt, Germany). Dulbecco's modified Eagle's medium (DMEM), fetal calf serum (FCS), horse serum (HS), L-glutamine, penicillin/streptomycin and trypsin were purchased from Biological Industries (Beth-Haemek, Israel). Methylthiazolyl blue (MT) was purchased from Chem-Impex International (Wood Dale, IL, USA). DMSO, EGTA, IGEPAL, NaCl, PBS tablets, DCF, Tris·HCl and protease inhibitor cocktail for mammalian cells were purchased from Merk (Rehovot, Israel). The Nuclear Extract Kit and Nrf2-DNA binding activity kit were purchased from Active Motif (Carlsbad, CA, USA).

All synthetic procedures and spectroscopic characterization of described in the manuscript compounds are shown in Supporting Information.

Molecular modelling

Pharmacophore modelling

The structure-based pharmacophore model was generated using the LigandScout software package.[29] LigandScout is able

to generate the 3D pharmacophores from structural data of macromolecule–ligand complexes. The program is taking for the calculations: H-bond donors and acceptors as directed vectors, positive and negative ionizable areas, and finally lipophilic fragments represented by spheres. The LigandScout model is very selective due to including in the calculations spatial parameters about potentially inaccessible for any kind of interactions areas for any ligand. This important detail in the pharmacophore formation is taking into account any potential steric restrictions. Excluded volume spheres are also included to the model based on the coordinates defined by amino acids side chain atoms to depict the inaccessible areas for any potential ligand.[51] This pharmacophore model was used as a query in virtual screening of ZINC database using the Screen Library protocol, as implemented in LigandScout.

Docking simulation

Docking simulations were performed using Glide[52-54] as implemented in Maestro V9.0.[55] For docking into crystal structures, Glide's grid box was centered on the coordinates of the ligand in the complex. A docking grid was generated within the docking box and ligands were docked into the binding sites using Glide's Extra Precision (XP) option with default parameters.

Cell culture and viability assay

PC-12 cells were grown in DMEM with 10% FCS, 5% horse serum and 1% (v/v) penicillin/streptomycin/nystatin, maintained at 37 °C in a humidified 5% CO_2 incubator. The cells (10,000 cells/well) were plated in 96-well tissue-culture plates in the medium (100 mL) and incubated overnight for attachment. The compounds were added to the cells for either 2.5, 6 or 24 h before exposure to oxidative stress (GO or H_2O_2).

The cell viability was evaluated by an MTT assay.[57] The cells were incubated with 3-(4,5- dimethylthiazol-2-yl)-2,5-diphenyltetrazolium bromide (MTT) (2 mg/ml) in growth medium for 30 min at 37 °C. The medium was then aspirated, and DMSO was added to solubilize the colored crystals. The absorbance at 570 nm was measured in an ELISA reader. The amount of color produced is directly proportional to the number of viable cells.

Assay for reactive-oxygen species

Quantification of the formation rate of ROS was determined as previously described.[58] Briefly, the compounds were diluted at a ratio of 1:10 with 40 mm Tris (pH 7.4) and loaded with 10 μM of DCF (in methanol) for 15 min at 37 °C. After exposure to a solution containing 30% H_2O_2, the formation of the fluorescent-oxidized derivatives of the DCF was monitored in a cuvette holder (thermostatically maintained at 37 °C) as follows: DCF, excitation wavelength (488 nm) and emission wavelength (525 nm). The DCF formation was quantified from separate-standard curves in methanol (0.05–1 lm).

Luciferase assay

The assay was conducted as described.[59]

Subcellular fractionation

Cellular nuclear fraction was prepared from PC-12 cells using a Nuclear Extract Kit (Active Motif, Carlsbad, CA, USA). The protein concentration was determined by the Lowry protein assay.[60]

Nrf2-DNA binding activity

The activation of Nrf2 was investigated by quantifying the binding of Nrf2 to ARE using a binding kit (TransAM Nrf2 DNA; Active Motif) according to the manufacturer's instructions. Briefly, nuclear protein (5–20 μg) was incubated for 1 hour in a 96-well plate coated with ARE sequence oligonucleotide. The bound Nrf2 was captured by anti-Nrf2 antibody and visualized by colorimetric reaction using secondary antibody. The resultant color was measured spectrophotometrically at 450/655 nm.

Statistical analysis

In vitro results are given as mean±SE. The statistical significance ($p < 0.05$) was calculated among the experimental groups using the two-tailed Student's t-test. The QuickCalcs online service Graph-Pad Software, found at www.graphpad.com/quickcalcs/ttest1.cfm, was used for statistical evaluations.

Acknowledgements

This study was supported by a Bar-Ilan University new faculty grant for A.G. Bar-Ilan University, Ramat Gan and Rabin Medical Center, Petah-Tikva, both in Israel, provided a grant for A.G and D.O. (Collaborative Grant in Biomedical Research – 2013). In addition, S. K. is thankful for the support of her work by the Wolf Foundation. We would like to thank Nechama-Sara Cohen for the English editing of the manuscript.

Keywords: Keap1 • Nrf2 • oxidative stress • oxopyrrolidine derivatives • computer modelling

References:

[1] E. Birben, U. M. Sahiner, C. Sackesen, S. Erzurum, O. Kalayci, *World Allergy Organ J*. **2012**, *5*, 9-19.

[2] M. Valko, K. Jomova, C. J. Rhodes, K. Kuca, K. Musilek, *Arch Toxicol*. **2016**, *90*, 1-37.

[3] X. Wang, C. Hai, *Mol Biol Rep*. **2016**, *43*, 607-628.

[4] M. Rutkowski, T. Matuszewski, J. Kedziora, M. Paradowski, K. Klos, A. Zakrzewski, *Pol Merkur Lekarski*. **2010**, *29*, 377-381.

[5] O. Blokhina, E. Virolainen, K. V. Fagerstedt, *Ann Bot*. **2003**, *91 Spec No,* 179-194.

[6] C. Espinosa-Diez, V. Miguel, D. Mennerich, T. Kietzmann, P. Sanchez-Perez, S. Cadenas, S. Lamas, *Redox Biol*. **2015**, *6*, 183-197.

[7] T. Nguyen, P. Nioi, C. B. Pickett, *J Biol Chem*. **2009**, *284*, 13291-13295.

[8] L. M. Zipper, R. T. Mulcahy, *J Biol Chem*. **2002**, *277*, 36544-36552.

[9] S. B. Cullinan, J. D. Gordan, J. Jin, J. W. Harper, J. A. Diehl, *Mol Cell Biol*. **2004**, *24*, 8477-8486.

[10] M. Furukawa, Y. Xiong, *Mol Cell Biol*. **2005**, *25*, 162-171.

[11] A. Kobayashi, M. I. Kang, H. Okawa, M. Ohtsuji, Y. Zenke, T. Chiba, K. Igarashi, M. Yamamoto, *Mol Cell Biol*. **2004**, *24*, 7130-7139.

[12] E. Kansanen, S. M. Kuosmanen, H. Leinonen, A.-L. Levonen, *Redox Biol*. **2013**, *1*, 45-49.

[13] K. Itoh, J. Mimura, M. Yamamoto, *Antioxid Redox Signal*. **2010**, *13*, 1665-1678.

[14] D. D. Zhang, S. C. Lo, J. V. Cross, D. J. Templeton, M. Hannink, *Mol Cell Biol*. **2004**, *24*, 10941-10953.

[15] T. W. Kensler, N. Wakabayashi, S. Biswal, *Annu Rev Pharmacol Toxicol*. **2007**, *47*, 89-116.

[16] T. Suzuki, H. Motohashi, M. Yamamoto, *Trends Pharmacol Sci*. **2013**, *34*, 340-346.

[17] Z. Hochberg, *Sci Signal*. **2010**, *3*, pt1.

[18] W. Li, S. Yu, T. Liu, J. H. Kim, V. Blank, H. Li, A. N. Kong, *Biochim Biophys Acta*. **2008**, *1783*, 1847-1856.

[19] S. K. Niture, J. W. Kaspar, J. Shen, A. K. Jaiswal, *Toxicol Appl Pharmacol*. **2010**, *244*, 37-42.

[20] M. Zhang, C. An, Y. Gao, R. K. Leak, J. Chen, F. Zhang, *Prog Neurobiol*. **2013**, *100*, 30-47.

[21] P. Canning, F. J. Sorrell, A. N. Bullock, *Free Radic Biol Med*. **2015**, *88*, 101-107.

[22] H.-P. Sun, Z.-Y. Jiang, M.-Y. Zhang, M.-C. Lu, T.-T. Yang, Y. Pan, H.-Z. Huang, X.-J. Zhang, Q.-d. You, *MedChemComm*. **2014**, *5*, 93-98.

[23] L. Hu, S. Magesh, L. Chen, L. Wang, T. A. Lewis, Y. Chen, C. Khodier, D. Inoyama, L. J. Beamer, T. J. Emge, J. Shen, J. E. Kerrigan, A. N. Kong, S. Dandapani, M. Palmer, S. L. Schreiber, B. Munoz, *Bioorg Med Chem Lett*. **2013**, *23*, 3039-3043.

[24] Z. Y. Jiang, M. C. Lu, L. L. Xu, T. T. Yang, M. Y. Xi, X. L. Xu, X. K. Guo, X. J. Zhang, Q. D. You, H. P. Sun, *J Med Chem*. **2014**, *57*, 2736-2745.

[25] E. Jnoff, C. Albrecht, J. J. Barker, O. Barker, E. Beaumont, S. Bromidge, F. Brookfield, M. Brooks, C. Bubert, T. Ceska, V. Corden, G. Dawson, S. Duclos, T. Fryatt, C. Genicot, E. Jigorel, J. Kwong, R. Maghames, I. Mushi, R. Pike, Z. A. Sands, M. A. Smith, C. C. Stimson, J.-P. Courade, *ChemMedChem*. **2014**, *9*, 699-705.

[26] D. Marcotte, W. Zeng, J.-C. Hus, A. McKenzie, C. Hession, P. Jin, C. Bergeron, A. Lugovskoy, I. Enyedy, H. Cuervo, D. Wang, C. Atmanene, D. Roecklin, M. Vecchi, V. Vivat, J. Kraemer, D. Winkler, V. Hong, J. Chao, M. Lukashev, L. Silvian, *Bioorg Med Chem*. **2013**, *21*, 4011-4019.

[27] R. Hancock, H. C. Bertrand, T. Tsujita, S. Naz, A. El-Bakry, J. Laoruchupong, J. D. Hayes, G. Wells, *Free Radic Biol Med*. **2012**, *52*, 444-451.

[28] D. D. Zhang, M. Hannink, *Mol Cell Biol*. **2003**, *23*, 8137-8151.

[29] G. Wolber, T. Langer, *J Chem Inf Model*. **2005**, *45*, 160-169.

[30] B. K. Shoichet, *Nature*. **2004**, *432*, 862-865.

[31] L. A. Greene, A. S. Tischler, *Proc Natl Acad Sci U S A*. **1976**, *73*, 2424-2428.

[32] A. M. Bokare, A. K. Praveenkumar, M. Bhonde, Y. Nayak, R. Pal, R. Goel, *Neurochem Res*. **2017**.

[33] H. Elkon, E. Melamed, D. Offen, *Cell Mol Neurobiol*. **2001**, *21*, 771-781.

[34] Y. Zhang, X. G. Gong, Z. Z. Wang, H. M. Sun, Z. Y. Guo, J. H. Hu, L. Ma, P. Li, N. H. Chen, *Eur J Neurosci*. **2016**, *43*, 1379-1388.

[35] I. Bobilev, V. Novik, I. Levi, O. Shpilberg, J. Levy, Y. Sharoni, G. P. Studzinski, M. Danilenko, *Cancer Biol Ther*. **2011**, *11*, 317-329.

[36] B. R. Imhoff, J. M. Hansen, *Cell Biol Toxicol*. **2010**, *26*, 541-551.

[37] P. L. Paytash, E. Sparrow, J. C. Gathe, *J. Am. Chem. Soc.* **1950**, *72*, 1415-1416.

[38] G. Guntas, S. M. Lewis, K. M. Mulvaney, E. W. Cloer, A. Tripathy, T. R. Lane, M. B. Major, B. Kuhlman, *Protein Eng Des Sel*. **2016**, *29*, 1-9.

[39] A. V. Kolobov, S. T. Panfilov, E. R. Kofanov, *Bashkirskii Khimicheskii Zhurnal*. **2006**, *13*, 168-169.

[40] K. Rutkauskas, V. Mickevicius, K. Kantminiene, M. Stasevych, O. Komarovska-Porokhnyavets, R. Musyanovych, V. Novikov, *Chemija*. **2013**, *24*, 74-80.

[41] K. Rutkauskas, E. Jakiene, Z. J. Beresnevicius, *Chemine Technologija*. **2003**, 68-73.

[42] M. Eckshtain-Levi, R. Lavi, D. S. Yufit, B. Daniel, O. Green, O. Fleker, M. Richman, S. Rahimipour, A. Gruzman, L. Benisvy, *Chem Commun (Camb)*. **2016**, *52*, 2350-2353.

[43] N. Kozlovsky, A. Rudich, R. Potashnik, N. Bashan, *Free Radical Bio Med*. **1997**, *23*, 859-869.

[44] A. Barzegar, *Mol Biol Res Commun*. **2016**, *5*, 87-95.

[45] R. Shapira, S. Rudnick, B. Daniel, O. Viskind, V. Aisha, M. Richman, K. R. Ayasolla, A. Perelman, J. H. Chill, A. Gruzman, S. Rahimipour, *J Med Chem*. **2013**, *56*, 6709-6718.

[46] J. D. Yeo, M. K. Jeong, C. U. Park, J. Lee, *Journal of Food Science*. **2010**, *75*, C258-262.

[47] W. Hur, Z. Sun, T. Jiang, D. E. Mason, E. C. Peters, D. D. Zhang, H. Luesch, P. G. Schultz, N. S. Gray, *Chemistry & biology*. **2010**, *17*, 537-547.

[48] H. Erlank, A. Elmann, R. Kohen, J. Kanner, *Free Radic Biol Med*. **2011**, *51*, 2319-2327.

[49] R. Sirota, D. Gibson, R. Kohen, *Redox Biol*. **2015**, *4*, 48-59.

[50] B. G. Richardson, A. D. Jain, T. E. Speltz, T. W. Moore, *Bioorg Med Chem Lett*. **2015**, *25*, 2261-2268.

[51] M. Rella, C. A. Rushworth, J. L. Guy, A. J. Turner, T. Langer, R. M. Jackson, *J Chem Inf Model*. **2006**, *46*, 708-716.

[52] R. A. Friesner, R. B. Murphy, M. P. Repasky, L. L. Frye, J. R. Greenwood, T. A. Halgren, P. C. Sanschagrin, D. T. Mainz, *J Med Chem*. **2006**, *49*, 6177-6196.

[53] T. A. Halgren, R. B. Murphy, R. A. Friesner, H. S. Beard, L. L. Frye, W. T. Pollard, J. L. Banks, *J Med Chem*. **2004**, *47*, 1750-1759.

[54] R. A. Friesner, J. L. Banks, R. B. Murphy, T. A. Halgren, J. J. Klicic, D. T. Mainz, M. P. Repasky, E. H. Knoll, M. Shelley, J. K. Perry, D. E. Shaw, P. Francis, P. S. Shenkin, *J Med Chem*. **2004**, *47*, 1739-1749.

[55] Schrödinger. **2009**.

[56] M. De Rosa, G. Vigliotta, G. Palma, C. Saturnino, A. Soriente, *Molecules*. **2015**, *20*, 22044-22057.

[57] A. Munder, L. L. Israel, S. Kahremany, R. Ben-Shabat-Binyamini, C. Zhang, M. Kolitz-Domb, O. Viskind, A. Levine, H. Senderowitz, S. Chessler, J. P. Lellouche, A. Gruzman, *ACS Appl Mater Interfaces*. **2017**, *9*, 1189-1206.

[58] C. P. Le Bel, H. Ischiropoulos, S. C. Bondy, *Chem Res Toxicol*. **1992**, *5*, 227-231.

[59] Y. Riahi, Y. Sin-Malia, G. Cohen, E. Alpert, A. Gruzman, J. Eckel, B. Staels, M. Guichardant, S. Sasson, *Diabetes*. **2010**, *59*, 808-818.

[60] G. L. Peterson, *Anal Biochem*. **1977**, *83*, 346-356.

Figure 1: Structure of known Keap1–Nrf2 PPI inhibitors

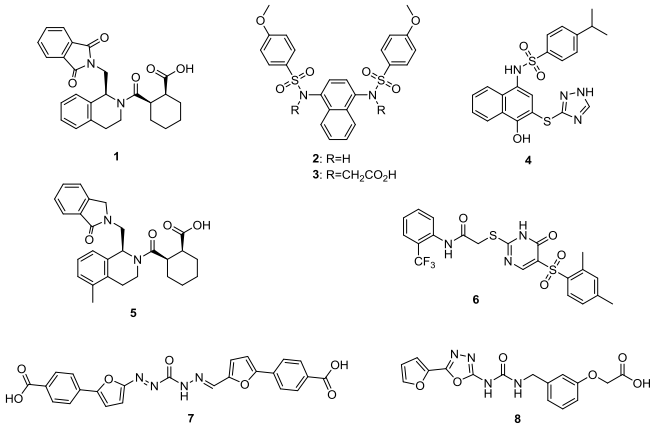

Figure 2: Pharmacophore design

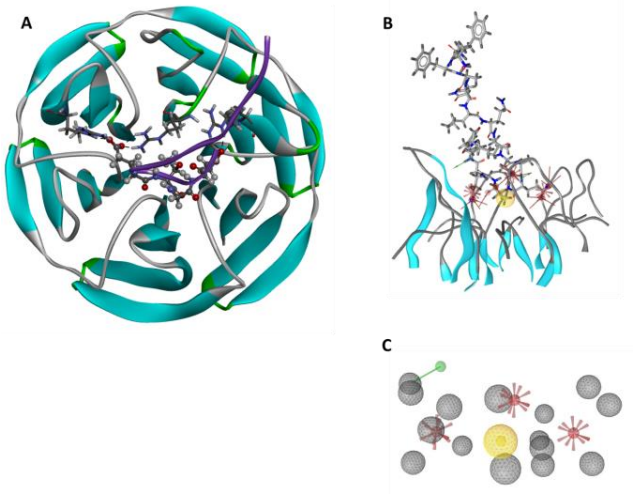

Figure 3: Virtual screening results

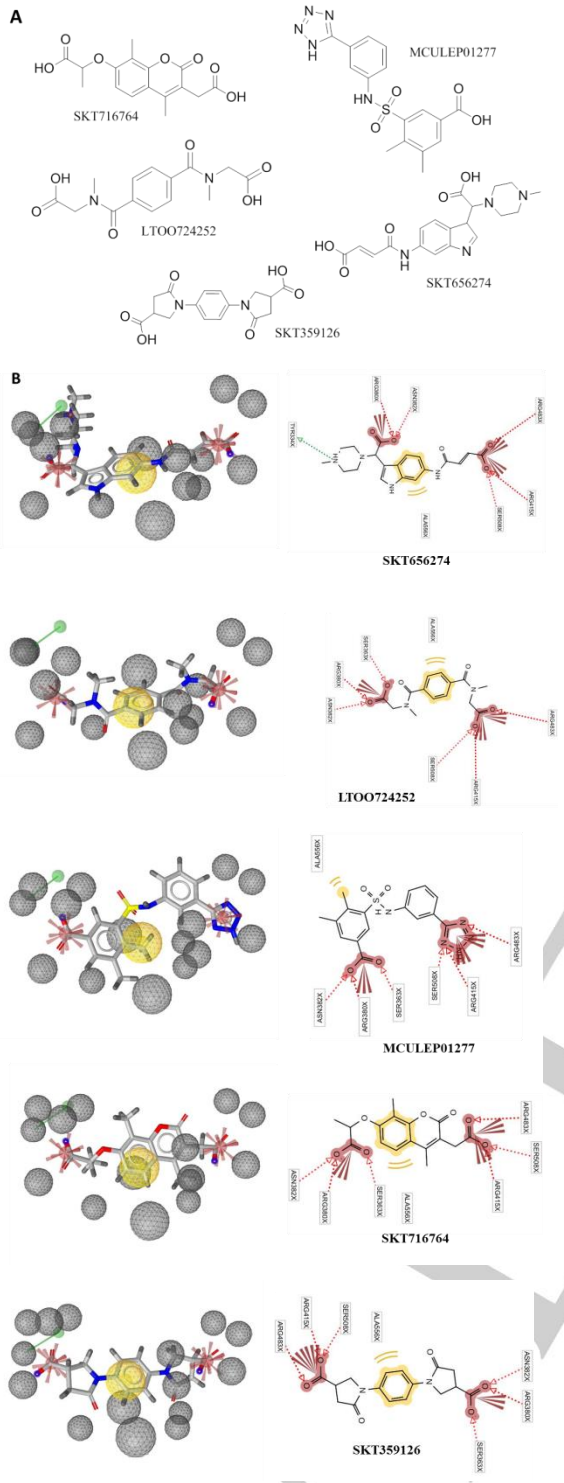

Figure 4: Docking of the five selected compounds at the Keap1 binding site and their 2D ligand interaction diagram

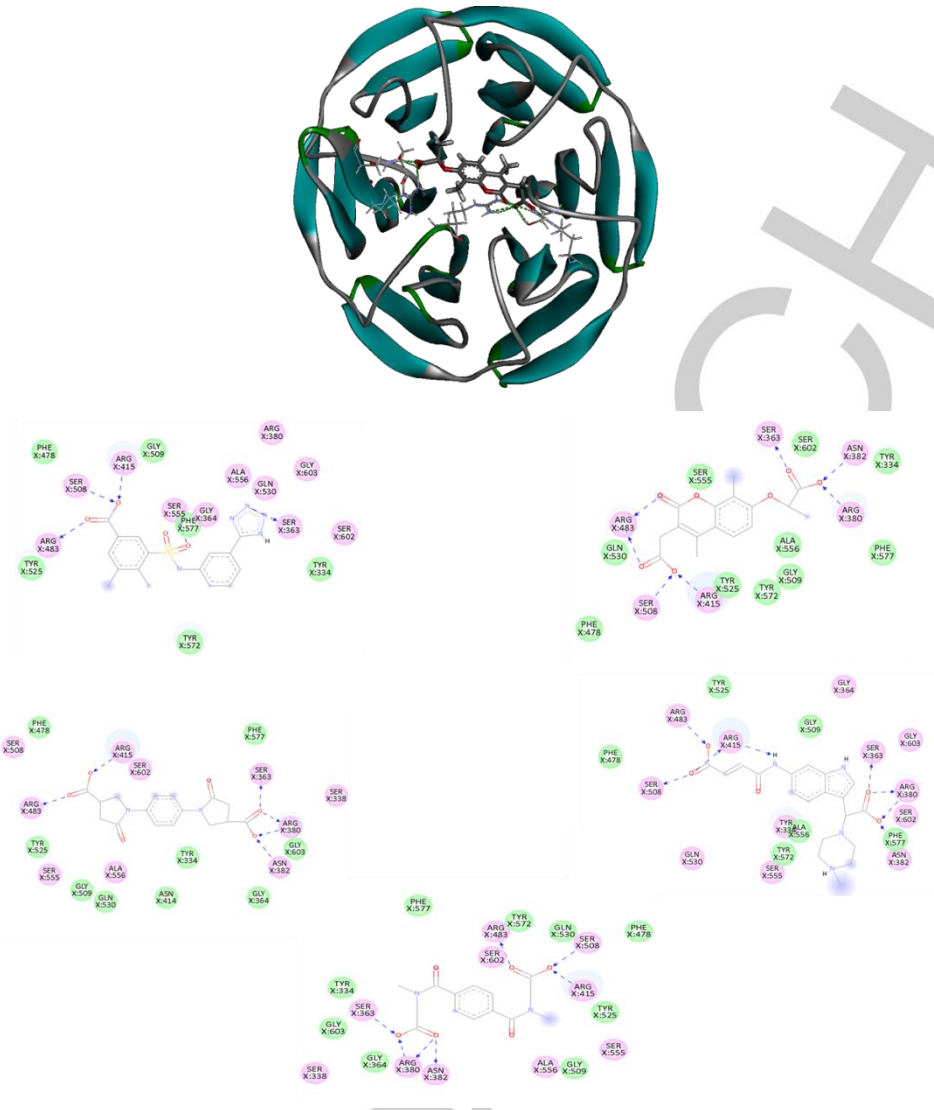

Figure 5: Screening of the five compounds with the highest fitting score

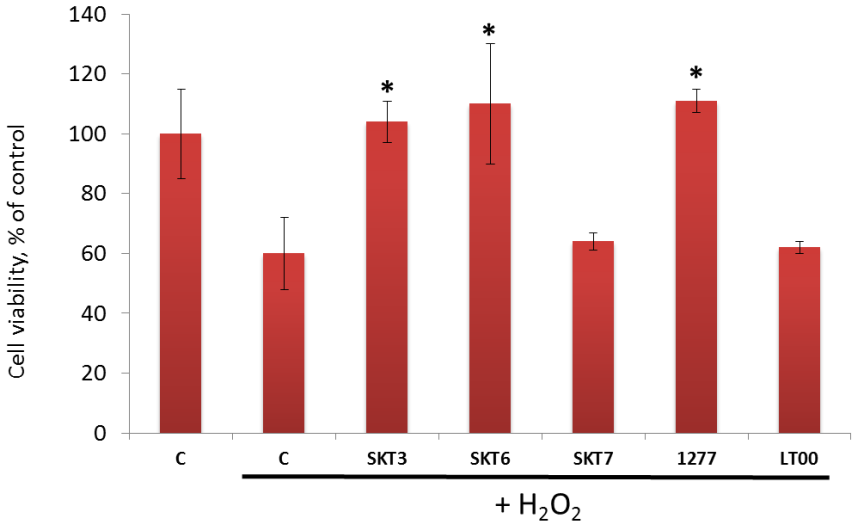

Figure 6: Stimulatory effect of SKT3 on the Nrf2 promoter

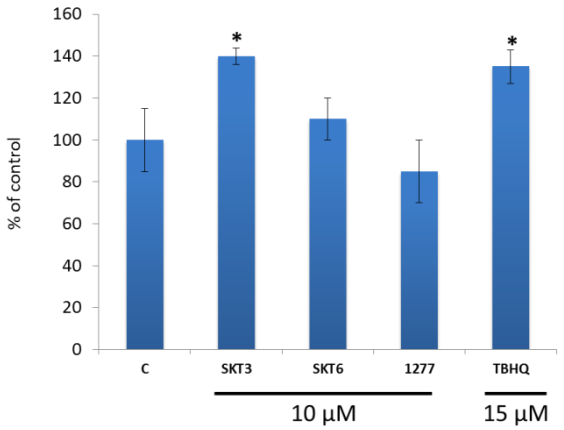

Figure 7: Effect of synthesized compounds on PC-12 viability

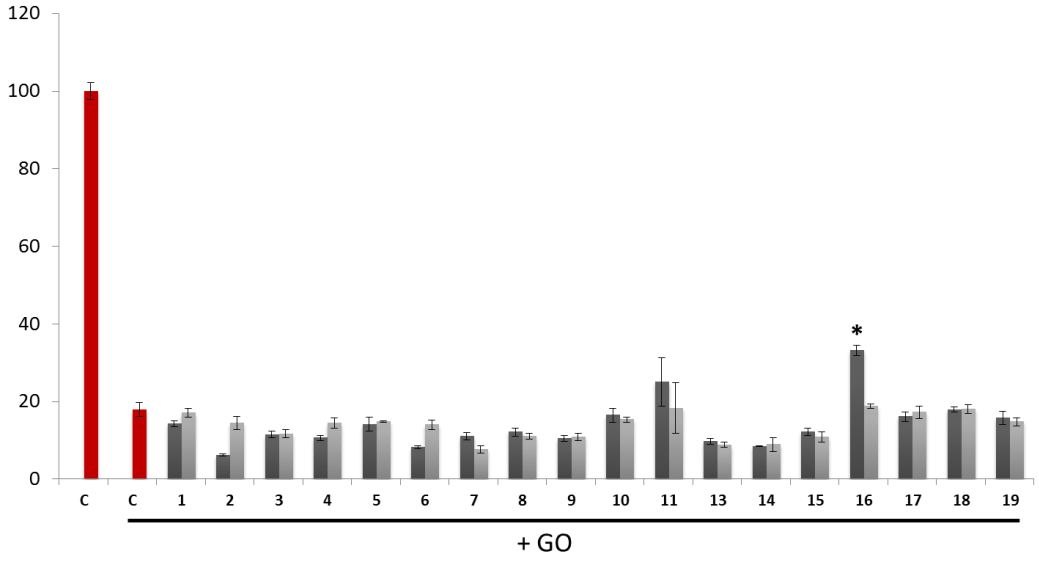

Figure 8: Pharmacological characterization of the lead compound

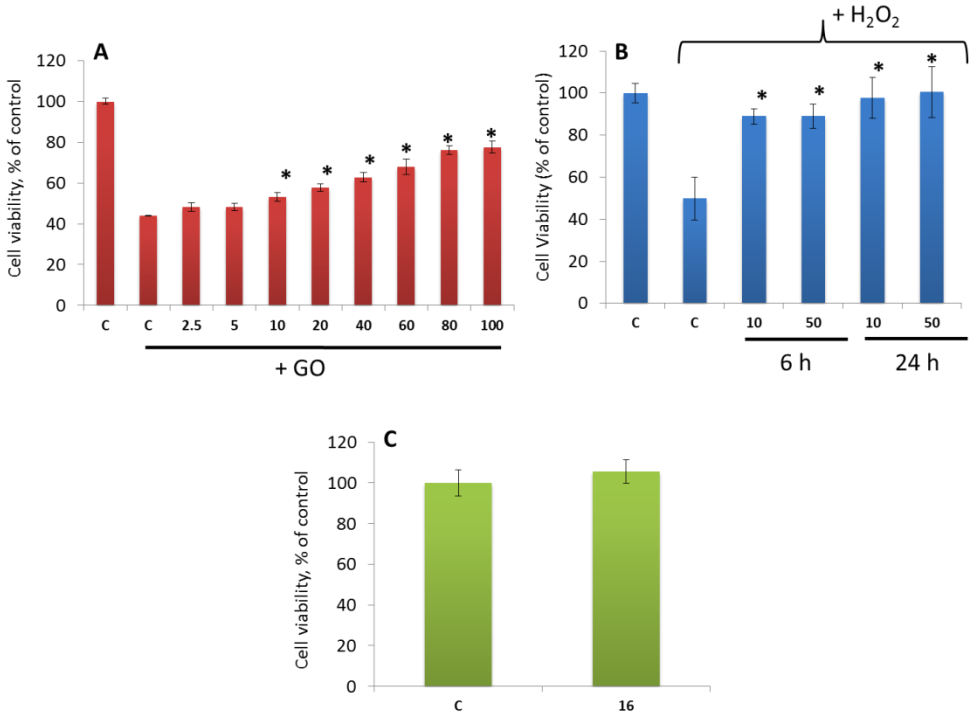

Figure 9: Dose-response analysis of the effect of **16** and its derivatives on PC-12 viability

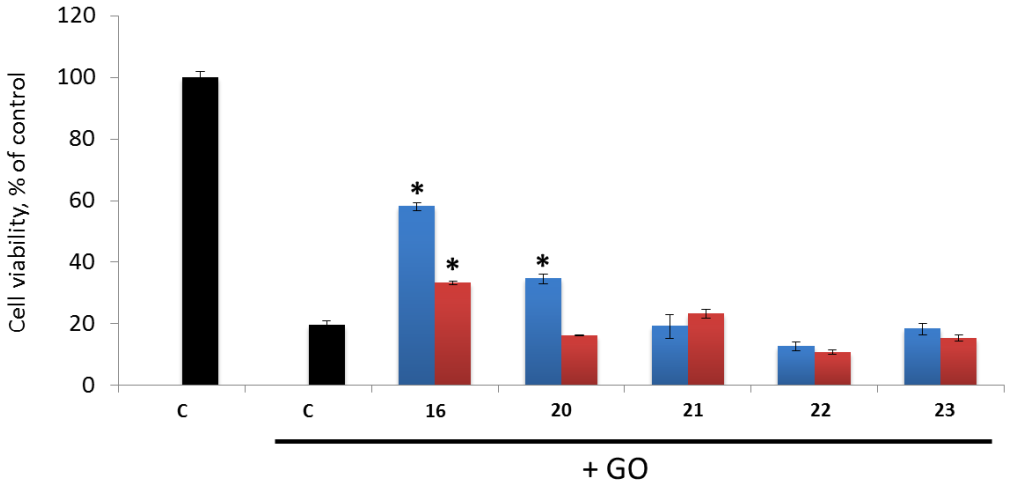

Figure 10: Lack of the DCF-scavenging effect of the test compounds

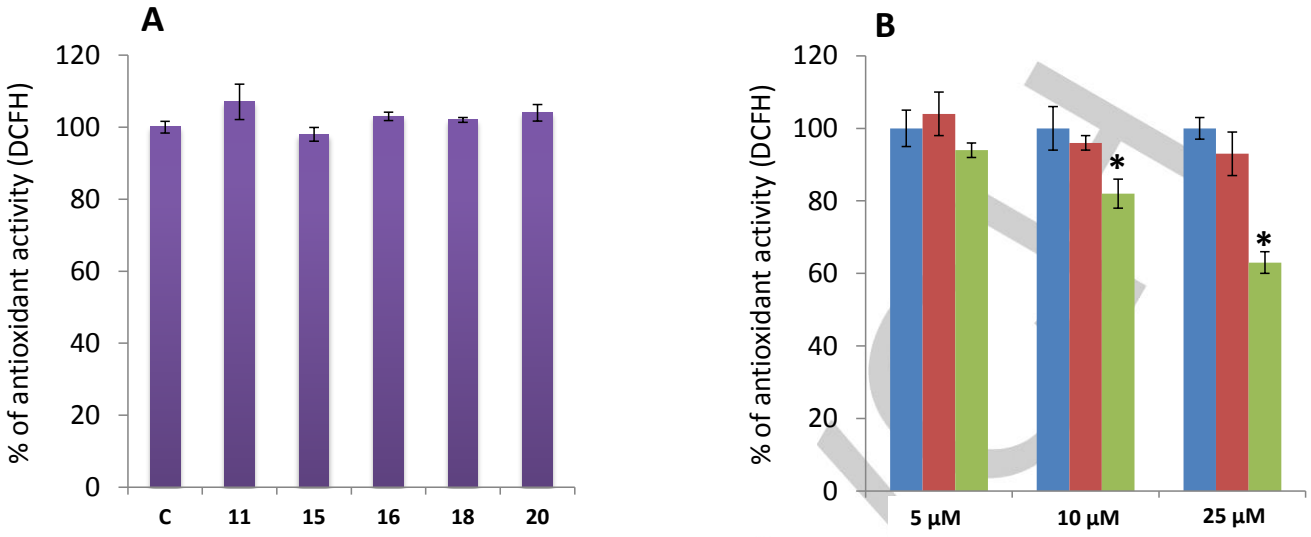

Figure 11: Compound **16** activates the Nrf2 anti-oxidant system

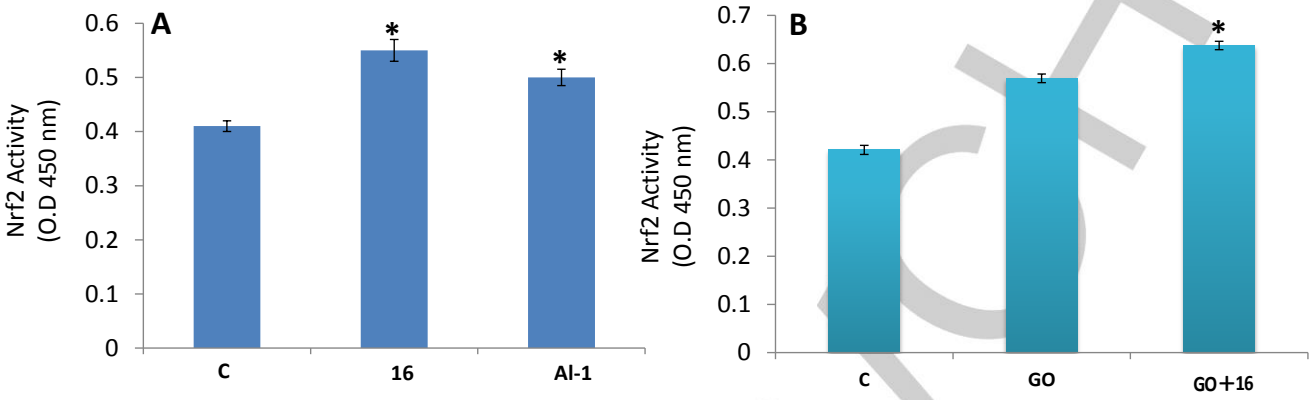

Figure 12: The binding mode between the active conformation of compound **16** and Keap1 provided by the Glide docking

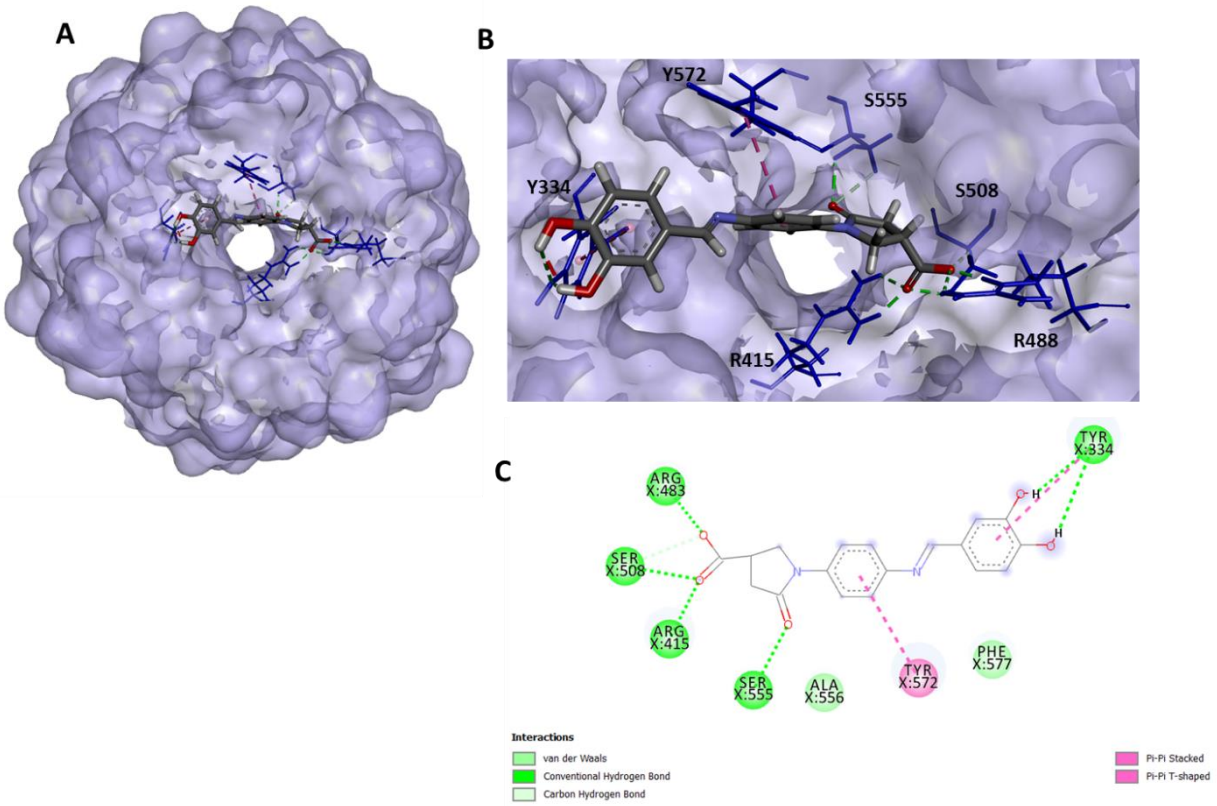

Scheme 1: Synthesis of nine novel amide pyrrolidine derivatives

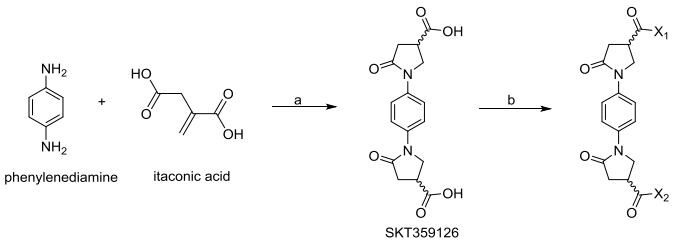

Compound	X_1	X_2
1	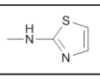	
2	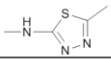	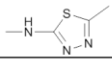
3	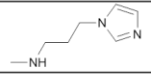	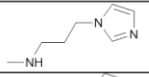
4	—OH	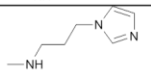
5	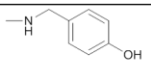	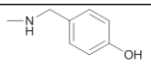
6	—OH	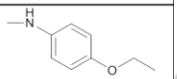
7		
8	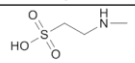	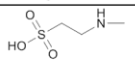
9	—OH	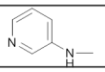

Scheme 2: Synthesis of **10** and **11**

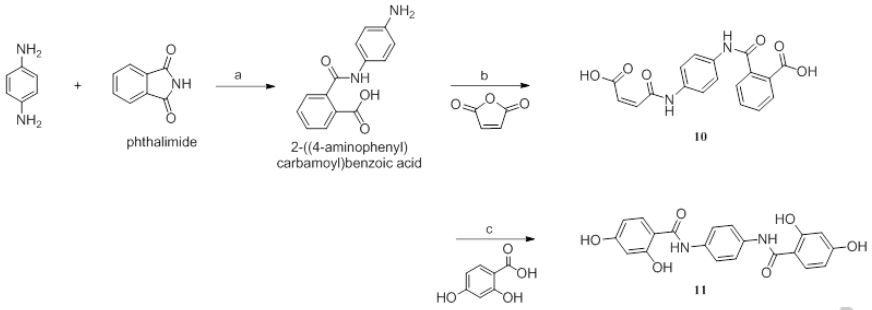

Scheme 3: Synthesis of **13**–**19**

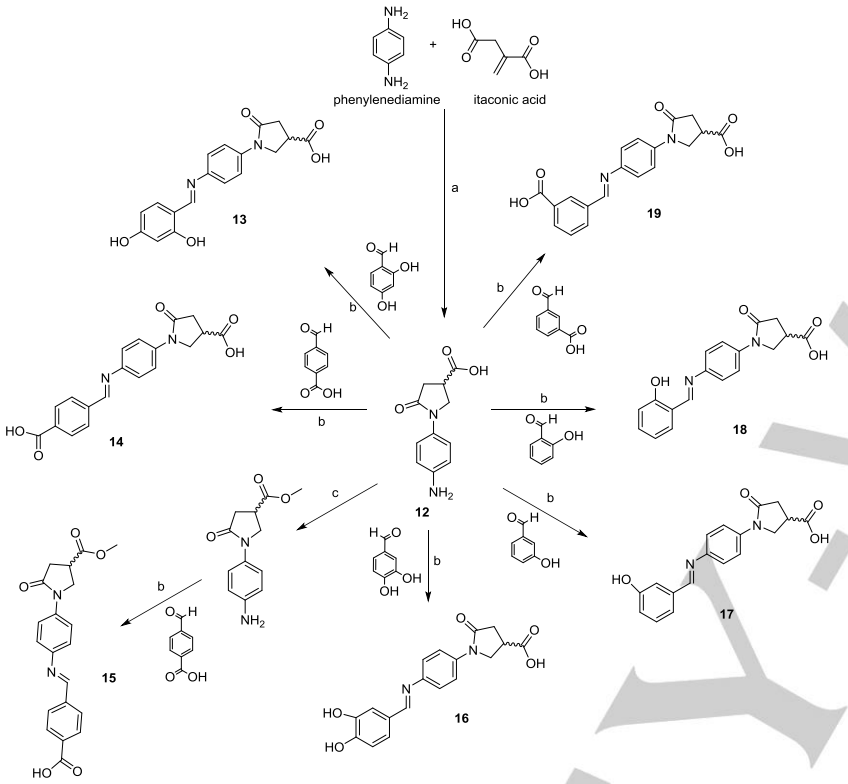

Scheme 4: Synthesis of **20**–**23**

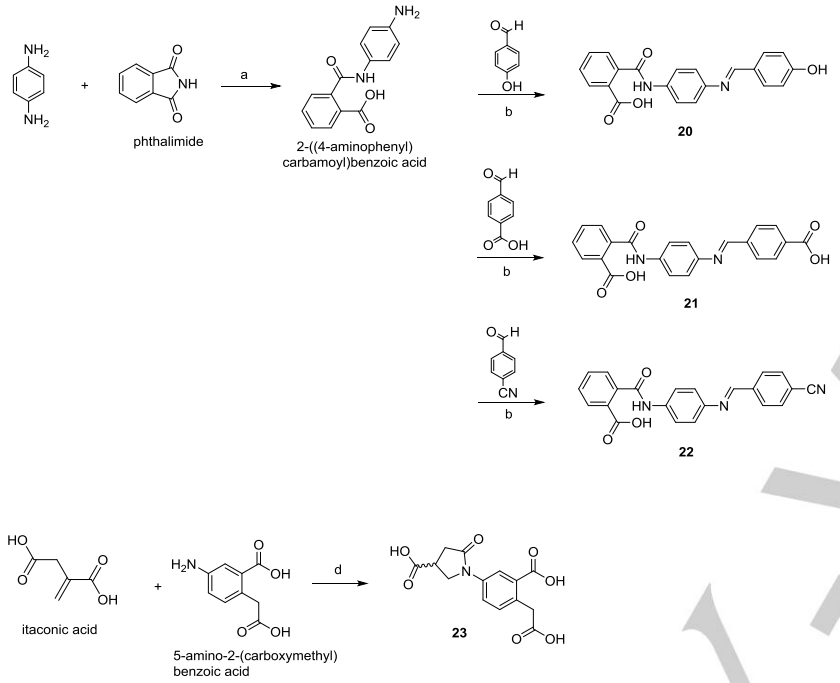

Entry for the Table of Contents

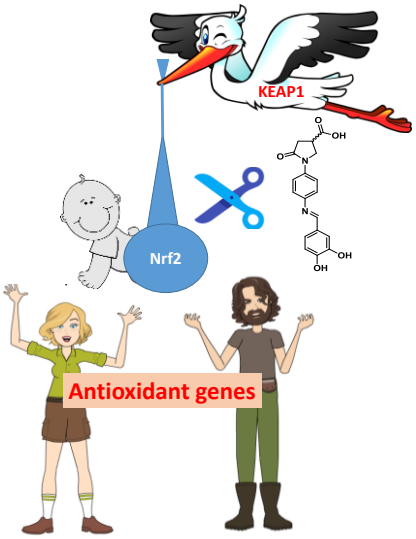

Using a structure-based virtual screening and the lead optimization, compound **16** (1-(4-((3,4-dihydroxybenzylidene)amino)phenyl)-5-oxopyrrolidine-3-carboxylic acid) was synthesized. The compound activated the Nrf2 transduction pathway in a dose- and time-dependent manner and protected P-12 cells against oxidative stress. A **16** can serve as a starting point for the development of therapeutics for the treatment of oxidative stress-related diseases.